AIChE

Measurement and Simulation of Flow Properties of Coal Ash Slag in Coal Gasification

Wenjia Song, Yimin Sun, Yongqiang Wu, and Zibin Zhu
The State Key Laboratory of Chemical Engineering, East China University of Science and Technology, Shanghai 200237, People's Republic of China

Shuntarou Koyama
Japan Coal Energy Center, Tokyo 108-0073, Japan

DOI 10.1002/aic.12293
Published online May 24, 2010 in Wiley Online Library (wileyonlinelibrary.com).

The viscosities of 45 coal ash slag samples at high temperature have been measured under different temperatures and shear rates. The computer thermodynamic software package FactSage has been used to predict liquidus temperatures, volume fractions of crystallized solid particles (ϕ), and the compositions of remaining liquid phase for 45 coal ash slag samples. The flow properties of completely liquid and partly crystallized coal ash slag samples have been predicted by three viscosity models. The Urbain formalism has been modified to describe the viscosities of fully liquid slag and homogeneous remaining liquid phase in coal ash slag samples. The modified Einstein equation and Einstein–Roscoe equation have been used to describe the viscosities of heterogeneous coal ash slag samples of $\phi < 10.00$ vol % and $\phi \geq 10.00$ vol %, respectively. These three models provided a good description of the experimental data of fully liquid and heterogeneous coal ash slag samples. The new models also predicted flow properties of mixtures of coal ash slags with CaO, Fe_2O_3, MgO, SiO_2, and Al_2O_3. © 2010 American Institute of Chemical Engineers *AIChE J,* 57: 801–818, 2011
Keywords: flow properties, coal ash slag, factsage, gasification

Introduction

Currently, coal provides more than 23% of the world's total primary energy and generates 41% of the world's electricity.[1] The consumption of coal for power generation is projected to increase by 49% by 2030.[2] However, the increased use of coal gives rise to several issues of serious environmental concern, including the increased release of greenhouse gas, particulars, and trace elements.[3] Therefore, there has been a significant increase in demand for more efficient and environmentally cleaner coal technologies for energy production.[4]

Conventional pulverized-fuel combustion is the most widely accepted technology for large-scale coal-fired heat and electricity generation. This technology, where the ash cannot contaminate the product, is used to generate stream through indirect heating.[5,6] The current development in next generation coal-fired power stations uses integrated gasification combined cycle (IGCC) technologies that address a number of problems on the increase of emissions of NO_x, SO_x, and particulates from pulverized coal-fired power stations. IGCC uses a combined cycle format with a gas turbine driven by the combusted syngas from the gasifier, whereas

Correspondence concerning this article should be addressed to Z. Zhu at zhuzb@ecust.edu.cn.

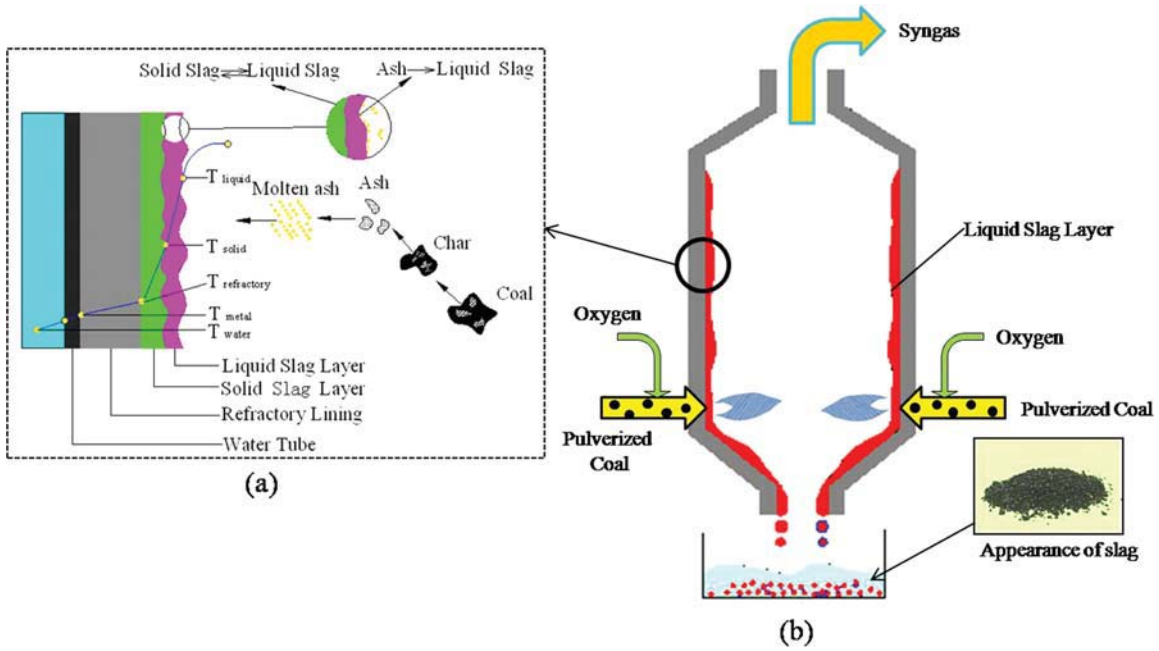

Figure 1. Slag deposit formation (a) and the slag tapping (b) schematic of the shell entrained-flow gasifier.

[Color figure can be viewed in the online issue, which is available at wileyonlinelibrary.com.]

the exhaust gases are heat exchanged with water/steam to generate superheated steam to drive a steam turbine, which can offer a basis for the development of low and ultimately zero emissions power generation technologies.[7] O_2/Steam-blown entrained-flow gasifiers have been successfully demonstrated in IGCC in Europe (Shell and Prenflo gasifier) and the United States (GE gasifier).[8] Meanwhile, the various entrained-flow gasifiers have been applied not only to IGCC but also to produce methanol and olefins (via methanol) in China.[9] However, the stable operations of entrained-flow gasifiers directly affect the stability and economic benefits of IGCC. Therefore, the entrained-flow gasifier plays an important role in the IGCC system.

In entrained-flow gasifiers, coal is typically gasified at high temperatures (>1200°C) and pressure (20–30 atm).[10] During gasification, organic material in coal is completely combusted and gasified under high-temperature and high-pressure conditions; the mineral matter in coal transforms into ash during coal combustion; and the ash exposed to high-temperature conditions, becomes liquid slag owing to the melting and reactions of its component mineral matter. Meanwhile, the molten ash particles accumulate on the internal walls of the gasification chamber, then the wall is covered by a layer of solid slag, over which the liquid slag will flow under the force of gravity and out of the bottom of the gasifier into a water quenching system.[11] Figure 1 schematically shows the typical slag deposit and the slag tapping of the shell entrained-flow gasifier. As a rule of thumb, the desirable slag viscosity at the tapping temperature should be 15–25 Pa s for entrained flow gasifier.[12] For example, if the viscosity of coal ash slag is above 25 Pa s, it will cause viscous, erratic slag flow from the gasifier; if the viscosity is below 5 Pa s, it will result in rapid refractory wear of the gasifier.[13] Thus, the viscosity of coal ash slag plays a key role in determining the operating conditions of entrained-flow gasifiers. As the operating temperature of the entrained-flow gasifiers is not necessarily above the liquidus temperature of coal ash slag, the liquid coal ash slag tapped from the gasifier is perhaps homogenous liquid slag or heterogeneous liquid slag containing crystallized particles.[14] It is, therefore, important to describe not only the viscosity of fully liquid phase but also the viscosity of the liquid phase containing the partly crystallized solid particles for coal ash slag in the gasifier.

It is known that measurements of the viscosity of coal ash slag at high temperature are experimentally difficult to carry out, laborious, expensive, and time-consuming.[15] Therefore, the ability to estimate viscosity data for coal ash slag is useful in coal gasification. There have been a number of studies on the viscosity prediction for coal ash slag at different temperatures.[16–20] As it can be assumed that the viscosity of the fully liquid phase of coal ash slag is of homogeneous liquid silicate slag, a number of silicate slag viscosity models have been developed over the years to predict the viscosity of fully liquid phase of coal ash slag.[21–24] One group of models uses a simplified expression based on the Weymann-Frenkel equation.[25]

$$\eta_l = ATe^{\left(\frac{1000B}{T}\right)} \tag{1}$$

where η_l is the viscosity of homogeneous liquid silicate, T is the absolute temperature, and A and B are the empirical parameters. Urbain et al.[26] indicated that parameters A and B depend on the molar fraction of silica. Jak et al.[27,28] modified the Weymann-Frenkel equation to be able to predict the viscosities of fully liquid phase slag for all compositions in the Al_2O_3–CaO–"FeO"–SiO_2 system in equilibrium with metallic iron and coal ash slag samples. Hurst et al.[29] fitted the

Table 1. The Composition of Coal Ash Samples

Number	Sample	Composition								
		SiO_2	Al_2O_3	CaO	Fe_2O_3	MgO	TiO_2	K_2O	Na_2O	S/A
1	LX	18.92	28.85	25.97	15.24	3.14	2.36	1.93	3.59	0.66
2	GJ	23.55	26.28	17.42	25.42	0.74	2.56	2.77	1.77	0.89
3	CL	33.54	31.28	6.94	13.55	7.12	2.75	1.92	2.89	1.07
4	HF	32.08	26.74	17.12	13.66	2.89	3.21	1.08	3.22	1.19
5	DT	36.94	30.78	16.21	9.12	3.12	0.38	2.11	1.34	1.20
6	PDS	30.18	24.46	6.02	36.94	1.04	0.63	0.56	0.17	1.23
7	GY	37.32	28.15	24.79	7.96	1.03	0.16	0.20	0.37	1.32
8	WL	42.74	31.79	6.53	11.77	1.86	1.83	1.30	2.10	1.34
9	AQ	41.91	30.97	13.24	9.15	0.28	1.02	2.92	0.51	1.35
10	XY	36.88	26.73	15.32	13.98	1.98	2.11	0.09	2.91	1.37
11	XLT	41.57	29.54	15.84	7.28	4.70	0.25	0.22	0.60	1.40
12	CC	51.51	35.72	4.92	3.78	1.62	1.05	0.80	0.59	1.44
13	GZ	43.57	29.83	14.09	8.57	1.20	0.22	1.32	1.20	1.46
14	SEK	39.85	26.85	15.1	14.3	3.14	0.38	0.13	0.53	1.48
15	YZ	27.17	16.98	15.36	38.22	1.16	0.42	0.19	0.51	1.60
16	SB	54.33	33.64	6.80	0.61	1.93	1.55	0.68	0.46	1.61
17	LEK	52.18	32.24	7.57	5.14	0.95	0.71	0.77	0.44	1.61
18	HM	38.62	23.71	9.12	20.84	2.90	2.27	0.43	2.10	1.62
19	SF2	45.95	27.21	152	6.77	1.55	1.51	1.21	0.60	1.68
20	CQ	45.47	26.73	6.74	16.96	0.44	2.08	1.12	0.44	1.70
21	GJW	53.16	30.31	5.60	4.42	3.00	1.27	1.63	0.59	1.75
22	JC	54.46	30.42	5.77	0.50	1.61	1.31	4.27	1.67	1.79
23	LW	47.11	26.32	18.10	2.33	0.62	1.26	0.61	3.65	1.79
24	YM	56.15	30.28	4.91	4.02	1.45	1.29	1.87	0.59	1.85
25	KL	38.24	20.13	28.97	4.31	3.32	1.91	2.11	1.01	1.89
26	DZ	44.55	23.45	14.94	13.06	1.16	1.32	1.30	0.22	1.89
27	HB	46.32	23.32	5.99	18.22	1.78	1.43	2.71	0.33	1.98
28	FH	53.19	26.2	8.76	6.63	1.53	1.51	1.66	0.53	2.03
29	HBL	27.05	12.79	38.44	16.85	1.76	0.83	0.78	1.49	2.11
30	ZZ	32.84	15.52	35.52	8.25	1.92	3.02	1.96	0.98	2.11
31	YB	48.91	22.91	6.18	18.11	1.25	1.70	0.61	0.33	2.13
32	HX	57.78	25.43	5.52	3.40	1.15	1.01	1.45	4.25	2.27
33	YC	46.42	20.14	4.26	25.52	0.73	0.99	0.27	1.68	2.30
34	XS	42.51	17.99	16.98	8.38	3.07	0.53	0.93	9.62	2.36
35	SF1	37.38	15.58	30.50	11.26	1.60	0.87	1.20	1.59	2.39
36	XZ	50.77	20.65	10.27	13.02	1.50	1.10	0.31	2.38	2.45
37	CJZ	45.55	18.22	15.62	14.38	3.00	1.33	1.90	0.88	2.50
38	DTU	47.70	19.08	14.87	9.12	2.12	3.33	1.02	2.76	2.50
39	FS	53.13	21.25	4.11	14.32	3.21	0.78	2.11	1.09	2.50
40	HX	42.31	16.77	20.18	11.79	7.08	0.70	0.43	0.74	2.52
41	SH	41.45	16.30	23.96	12.82	1.52	0.95	1.49	1.48	2.54
42	SM	34.06	13.38	36.50	9.17	1.93	1.01	0.12	3.81	2.54
43	ZLNE	35.31	13.48	31.60	13.49	2.43	0.71	0.17	2.80	2.61
44	LW	47.54	18.08	8.34	17.32	2.12	3.33	1.09	2.18	2.62
45	SX	46.11	17.26	9.12	24.06	0.67	0.86	0.29	1.63	2.67

viscosity of coal ash slag samples using the modified Weymann-Frenkel treatment to give separate models for the four FeO levels.

The other groups of more fundamental silicate viscosity models have also been developed using thermodynamic properties of the liquid phase silicate slag and internal structure of silicates through bridging, nonbridging, and free oxygens.[30,31] Seetharaman et al.[32] described a correlation between the Gibbs energy of activation for viscosities and the Gibbs energy of mixing for the silicate slag. Kondratiev et al.[33] linked the viscosity of homogeneous liquid phase silicate slag and the internal structure of melts through the concentration of various anion/cation structural units. The concentrations of structural units are equivalent to the second nearest neighbor bond concentrations calculated by the quasi-chemical thermodynamic model. Mill et al.[34] summarized and compared recently developed viscosity models in the ''round robin'' project.

For the heterogeneous coal ash slag containing some crystallized particles, fewer studies devoted to viscosity were found in literature.[35,36] More studies reported results for geological melts and artificial melts.[37,38] A number of empirical and semi-empirical viscosity models of heterogeneous liquid suspensions have been reviewed by Nzihou et al.[39] The most commonly used relationship describing the viscosity of heterogeneous molten coal ash slag is the Einstein–Roscoe type equation[40,41]:

$$\frac{\eta_s}{\eta_l} = \left(1 - \frac{\phi}{\phi_m}\right)^{-D} \tag{2}$$

where η_s is the viscosity of the crystallized particles containing coal ash slag; ϕ is the volume fraction of crystallized particles;

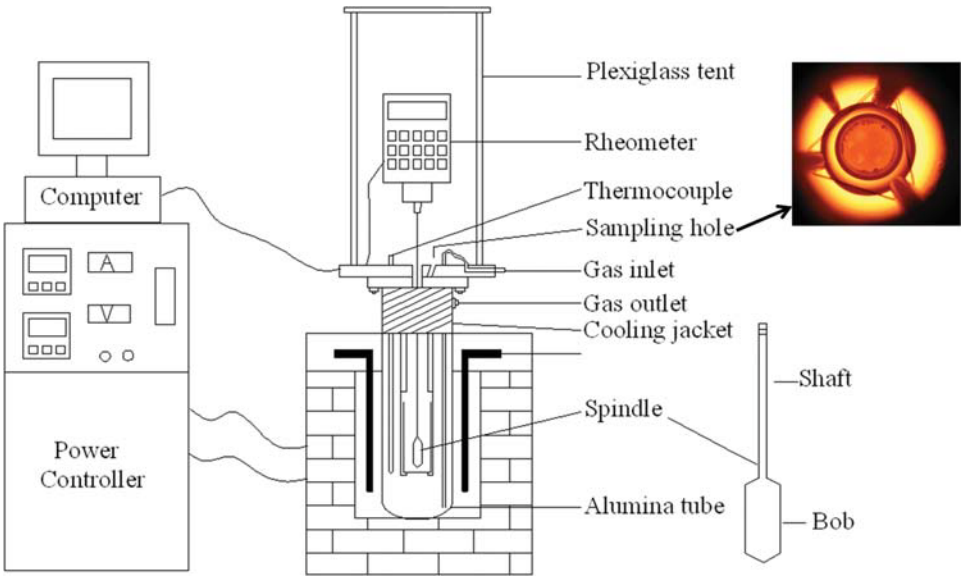

Figure 2. Setup for viscosity measurement.

[Color figure can be viewed in the online issue, which is available at wileyonlinelibrary.com.]

D is a constant; and ϕ_m represents the maximum amount of crystallized particles that the slag could accommodate before the viscosity becomes "infinite." For spherical particles of a uniform size, Roscoe[41] suggested D and ϕ_m to be 2.5 and 1.35, respectively. Kondratiev et al.[28] applied the Einstein–Roscoe equation to describe the effect of the presence of solid suspension on the viscosity of partly crystallized coal ash slag. Wright et al.[42] modified the D and ϕ_m parameters in the Einstein–Roscoe equation to fit the viscosities of geological slags containing particles of different shapes.

Other authors[43] also expressed the viscosity of heterogeneous coal ash slag in the form of the following power series:

$$\eta_s = \eta_l(1 + 2.5\phi + 9.15\phi^2) \quad (3)$$

However, Oh et al.[44] believed these models were valid only for very small concentrations of crystallized particles but could not describe the effect of shear rate on the viscosity.

In the work described in this article, we have measured the viscosities of 45 coal ash slag samples using a high-temperature rheometer at different temperatures under various shear rates. The three different viscosity models that predicted the viscosity of coal ash slag samples at various solid contents and temperatures were developed in conjunction with the computer thermodynamic software package FactSage. FactSage was used to predict liquidus temperatures, volume fractions of crystallized solid particles (ϕ), and the compositions of remaining liquid phase. Examples of the application of these models given in this article are concerned with prediction viscosity and temperature of critical viscosity (T_{cv}) of the mixtures of coal ash slag with various oxides.

Experimental

Coal ash sample

A total of 45 representative Chinese coal samples were used in the study. The ash samples were prepared in a muffle furnace at 815°C for 24 h according to the Chinese standard GB/T 1574-1995. Chemical analysis of the samples was carried out using X-ray fluorescence (XRF). The chemical composition of the 45 coal ash samples is given in Table 1.

Viscosity measurements

Apparatus. The high-temperature rheometer constructed for this research was designed for direct measurement of the rheological properties of slag in a controlled environment at

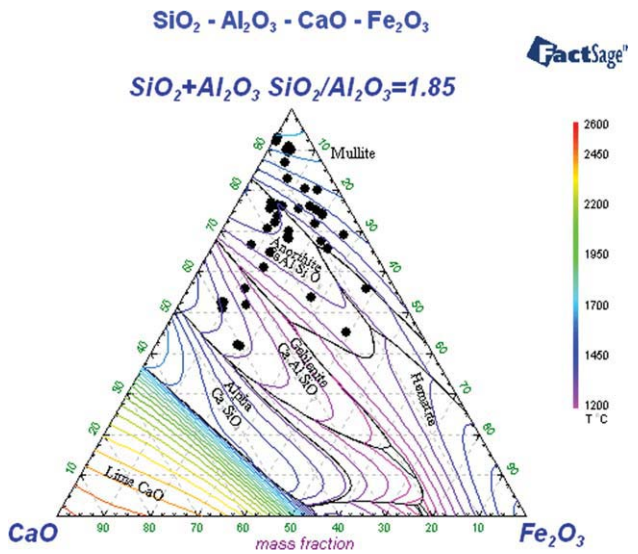

Figure 3. Liquidus surface in the system Si–Al–Ca–Fe–O with S/A weight ratio of 1.85 (calculated by FactSage) and bulk compositions of coal ash samples under investigation simplified to the four component system.

[Color figure can be viewed in the online issue, which is available at wileyonlinelibrary.com.]

Table 2. The Homogenous Liquid Viscosity Model Parameters

	j	i			
		0	1	2	3
b_i^0	0	12.72	35.11	−36	140.31
$b_i^{C,j}$	1	−4.01	24.75	−48.08	31.92
	2	3.75	−21.09	35.35	−19.93
$b_i^{M,j}$	1	−16.83	80.76	−121.68	58.21
	2	24.18	−116.15	178.12	−88.01
$b_i^{K,j}$	1	12.29	68.72	122.47	−66.31
	2	−6.41	21.43	−1.54	−88.01
$b_i^{N,j}$	1	10.76	−31.58	−10.17	60.29
	2	−10.41	−1.26	138.46	−190.67
$b_i^{T,j}$	1	27.56	−127.6	198.61	−104.08
	2	−34.77	165.31	−272.92	157.67

temperatures in the range 500–1570°C. The equipment and its essential components are shown schematically in Figure 2. This apparatus was set up at the East China University of Science and Technology. The rheometer employs a concentric cylindrical system for rheological measurements. The principle of operation of the high-temperature rheometer is to drive a spindle (which is immersed in the molten liquid slag) through a calibrated spring in the Brookfield rheometer. The viscous drag of the slag against the spindle is measured by the spring deflection. Spring deflection is measured with a rotary transducer. The viscosity measurement range of the rheometer is determined by the rotational speed of the spindle, the size and shape of the spindle, the crucible the spindle is rotating in, and the full-scale torque of the calibrated spring.

A vertical-tube alumina furnace equipped with a microprocessor temperature controller is used to heat the slag to the required test temperature. The temperature of the slag in the hot zone and in the measuring system is monitored using type B platinum thermocouples. A Brookfield DV-III ultra programmable rheometer was used for the measurements and was controlled by a PC, through which the experimental data were collected and stored for on-line processing and analysis.

In our experiment, the spindle was fabricated from 8.90 mm high-purity alumina bar stock. The spindle was 8.90 mm long with a 30° tapper (to help the molten liquid slag drain off when the spindle is lifted from the liquid slag) attached on both ends. The top of the spindle ended in a 15.00-mm-long, 2.34-mm-diameter shaft that accommodated a 300 mm long, 4.00 mm-diameter stem. The stem was covered by a tubular alumina sleeve. The spindle was attached to the Brookfield rheometer measuring head with a rigid shaft. A crucible of internal diameter 30 mm and height 90 mm was used to store the slag, which was contained inside a larger crucible of internal diameter 40 mm and height 100 mm to prevent damage to the fluted rods from any overflow of boiling slag from the small crucible. Slag could be taken directly from the sampling hole of the high-temperature rheometer at any high temperature under oxidizing conditions (see Figure 2). It was then rapidly quenched in cold water to observe the crystalline particles that it contained.

The bob was calibrated against Brookfield standard oil with nominal viscosities of 5.00 Pa s, 30.00 Pa s, 60.00 Pa s, and100.00 Pa s at 25°C in the range of actual rotation rates and at high temperature with a standard reference material developed in the BCR (Bureau Communautaire de Référence) program of the EU (19.46% Li_2O, 14.06% Al_2O_3, and 63.8% SiO_2); the measured deviation from the mean was $\leq$10.00%. As both the bob and crucible were made of Al_2O_3, some dissolution of Al_2O_3 in the slag was inevitable, affecting the bob and crucible geometry and the composition of the slag. This may possibly have caused certain systematic uncertainties and experimental errors.

Viscosity Measurements. We placed the slag in a crucible, which was in turn placed inside a larger crucible as mentioned above. This dual-crucible system was placed in the furnace, fixed by three fluted rods of high-purity alumina to ensure that the spindle was at the center of the crucible.

Generally, viscosity measurements were started at the temperature 20°C higher than the liquidus temperature of the coal ash slag sample. If the liquidus temperature of the sample was higher than the highest temperature of the furnace (1570°C), the starting temperature would be the highest temperature of the furnace under this condition. Viscosity measurements were made at 20°C intervals with stirring during stepwise cooling until the slag viscosity exceeded 300 Pa s. About at least 60 min was allowed for equilibration at each temperature. Moreover, at each chosen temperature, the slag viscosity was measured several times at different spindle speeds to ensure the reproducibility of the measurements. The spindle speed and the slag viscosity were recorded and processed by the apparatus software. After each test run at a fixed temperature, a few of the slag samples were directly transferred from the sampling hole of the high-temperature rheometer and quickly quenched with cold water. The microstructures of the quenched slag samples were examined by means of an optical rheology microscope.

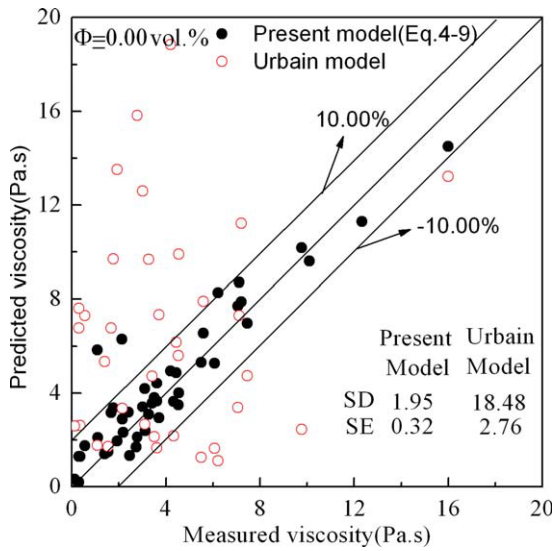

Figure 4. Comparison between the calculated viscosity values of fully liquid phase coal ash slag samples from the models and the experimental data.

[Color figure can be viewed in the online issue, which is available at wileyonlinelibrary.com.]

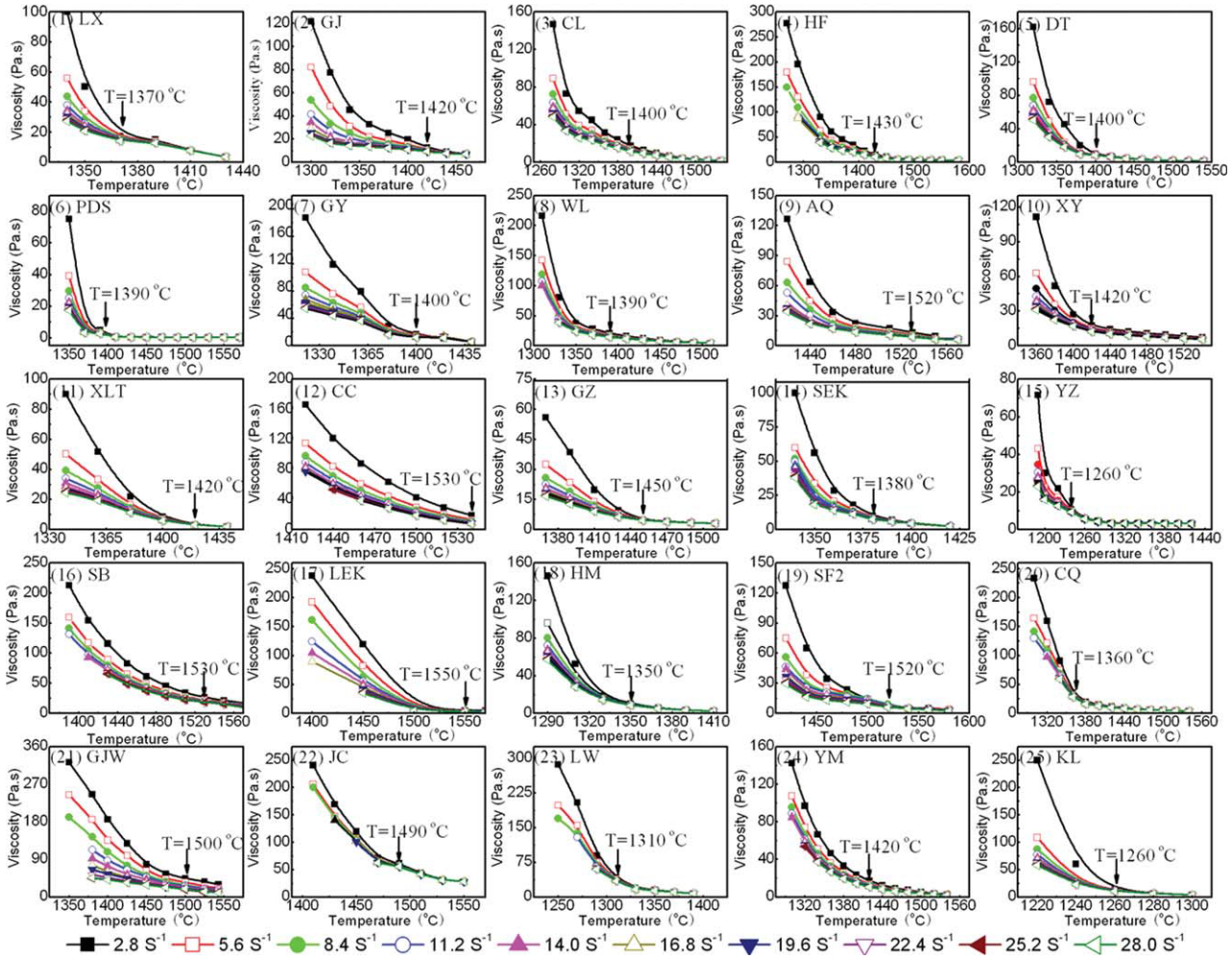

Figure 5. Viscosity vs. temperature curves for Nos. 1–25 coal ash slag samples at different shear rates.

[Color figure can be viewed in the online issue, which is available at wileyonlinelibrary.com.]

FactSage modeling

The thermodynamic software package FactSage[45] was used in this study to predict liquidus temperature, proportions of solids, and mineral formation for the multi-component system. Phase formation data for these oxides and their combinations were selected from the FToxid database. Calculations were carried out between solid temperature and liquid temperature under oxidizing condition at 1-atm pressure. The calculation method of FactSage is based on Gibbs' energy minimization for the slag at a given temperature and compositional range. Phases formed at concentrations below 0.01 wt % were ignored. Because of the complexity of the thermodynamic models (quasi-chemical, sub-lattice), which represents the interaction of the components for phase formation, the convergence of the algorithms is slow and sensitive. In this study, we used the method of Jak et al.,[18] which permits the approximation to start from lower order subsystems, finally reaching the real or complete system. Once the phases have been determined, a total mass balance verifies the consistency of the system.

In our work, the thermodynamic properties calculated for the slag by FactSage have been predicted from the (SiO_2–Al_2O_3–CaO–Fe_2O_3–MgO–TiO_2–Na_2O–K_2O) system. Liquid temperature of the slag was determined for the mineral matter that it contained.[46] On the basis of the oxide composition of the slag, the proportion of liquid phase generated and the compositions of remaining liquid phase were evaluated at different temperatures. FactSage is a thermodynamic equilibrium model. Thus, to allow the coal ash slag samples to reach thermodynamic equilibrium and eliminate the kinetic limitations of crystallized particles in coal ash slag at decreasing temperatures. The viscosity values of coal ash slag samples at different temperatures were used until the viscosity values of such samples no longer changed significantly with time.

Results and Discussion

Description of coal ash slag samples

A set of 45 coal ash slag samples was selected for this study and their chemical compositions are shown in Table 1.

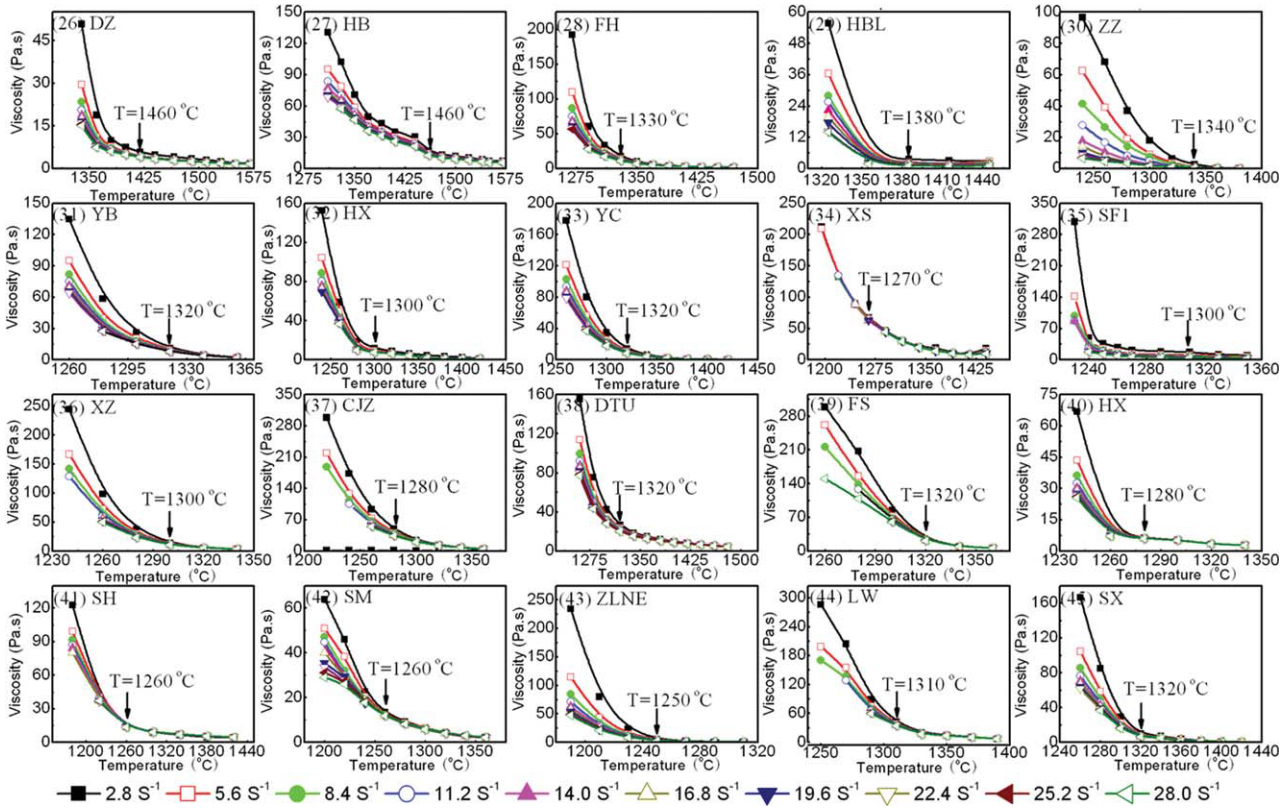

Figure 6. Viscosity vs. temperature curves for Nos. 26–45 coal ash slag samples at different shear rates.

[Color figure can be viewed in the online issue, which is available at wileyonlinelibrary.com.]

As can be seen from Table 1, the range of content of SiO_2, Al_2O_3, CaO, Fe_2O_3, MgO, TiO_2, K_2O, and Na_2O are 18.92–57.78%, 12.79–35.72%, 4.11–38.44%, 0.50–38.22%, 0.28–7.12%, 0.16–3.33%, 0.09–4.27%, and 0.17–9.62%, respectively, which basically cover the compositions of these oxides in most Chinese coal ash slags.[47,48]

To observe more directly the distribution of composition for these coal ash slag samples, we used FactSage to draw the pseudo-ternary diagram (SiO_2–Al_2O_3–CaO–Fe_2O_3 with an SiO_2/Al_2O_3 weight ratio of 1.7) in Figure 3. Since over 90% of the mineral matter in coal ash slag is derived from the oxides of aluminum, silicon, calcium, and iron, the SiO_2–Al_2O_3–CaO–Fe_2O_3 pseudo-ternary diagram can well describe the distribution of composition for these coal ash slag samples. In Figure 3, thick lines of the same color represent all compositions having a given liquidus temperature. The black point indicates a similar composition of coal ash slag samples. As shown in Figure 3, the compositions of most coal ash slag samples are located in the region containing mostly SiO_2 and Al_2O_3, where the coal ash slag samples have mullite as the first solid to precipitate and have high liquidus temperatures. High lime and high iron oxide coal ash slag samples have lower liquidus temperatures and are anorthite and Al–Fe–oxide primary phase fields, respectively. Note that actual S/A weight ratios in the set of coals investigated vary from 0.66 to 2.67; however, the SiO_2/Al_2O_3 (S/A) weight ratios of most coal ash slag samples were equal or close to 1.85 and the effects on liquidus temperature curves and mineral matter with the variation of the S/A weight ratio were negligible, thus we used the S/A weight ratio of 1.85 on behalf of all the samples in our experiment.

The viscosity model development

Development of the Viscosity Model for Homogeneous Coal Ash Slag. In our work, the experimental furnace temperature is usually higher than the liquidus temperature calculated by FactSage for coal ash slag samples, with the exception of five coal ash slag samples [PDS(6), AQ(9), LEK(17), DZ(26), and HB(27)]; These five coal ash slag samples whose liquidus temperatures are above the highest temperature of furnace (1570°C) are shown in Figures 7 and 8. Generally, a coal ash slag is heated up to the liquidus temperature until all reactions are completed; it will then normally form a homogenous liquid slag free of suspended matter,[49] thus the viscosities at the highest temperature for these 40 coal ash slag samples whose liquidus temperatures are lower than the highest temperature of furnace can be assumed to be that of fully liquid coal ash slag.

As the Urbain model[26] is one of the most widely used models for the completely liquid silicate slag viscosities due to its simplicity and good description of experimental data, it was selected as the basis for the description of viscosities of the fully liquid at highest temperature and the remaining liquid slag at different temperatures for all the coal ash slag samples.

The Urbain model uses modified expression based on the Weymann-Frenkel equation (Eq. 1). In Weymann-Frenkel equation, Urbain thought A and B were the model

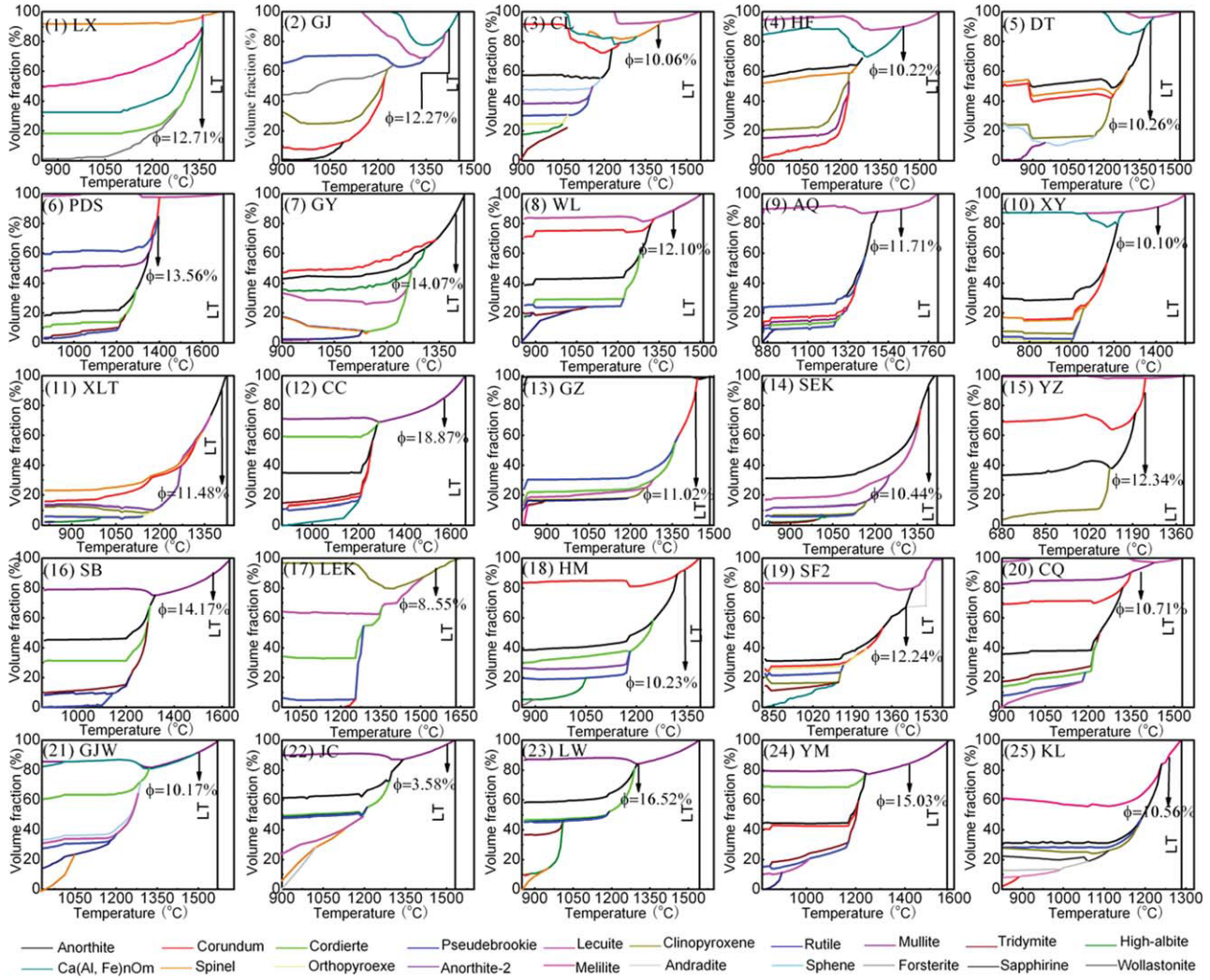

Figure 7. The volume fraction of liquid phase and crystallized solid particles and the mineral compositions for Nos. 1–25 coal ash slag samples at different temperatures.

[Color figure can be viewed in the online issue, which is available at wileyonlinelibrary.com.]

parameters, which depended only on the liquid silicate slag composition.

Parameter A is linked to B through the following empirical equation:

$$-\ln A = mB + n \tag{4}$$

where m and n are the model parameters.

Urbain[50] indicated that parameters m and n depended on composition, but for simplicity, recommended the average values $m = 0.29$ and $n = 11.57$ for the whole range of liquid silicate slag compositions.

The silicate liquid slag components are classified into three groups: glass formers (e.g., SiO_2)—g, amphoterics former (Al_2O_3, Fe_2O_3)—am, and modifier former (CaO, MgO, TiO_2, K_2O, Na_2O)—mo.[51] Thus, parameter B was expressed by Urbain as follows: function of glass former X_g (e.g., Si^{4+}), modifiers X_{mo} (e.g., Ca^{2+}, Mg^{2+}, Ti^{4+}, K^+, Na^+), and amphoterics X_{am} (e.g., Al^{3+}, Fe^{3+}):

$$B = B_0 + B_1 X_g + B_2 X_g^2 \tag{5}$$

where

$$B_{i=0\ldots3} = b_i^0 + b_i^1 a + b_i^2 a^2 \tag{6}$$

$$a = \frac{X_{mo}}{X_{mo} + X_{am}} \tag{7}$$

In the above Eqs. 5–7, X_g, X_{mo}, and X_{am} are mole fractions of glass formers (g), modifiers (mo), and amphoteric oxides (am), respectively. Meanwhile, b_i^j are empirical model parameters.

For systems containing more than one modifier, Urbain[52] proposed that separate B values for different individual modifiers be used. Although modified B-values by different modifiers had been presented,[34,50,51] these modifications have not been previously implemented. In the present study,

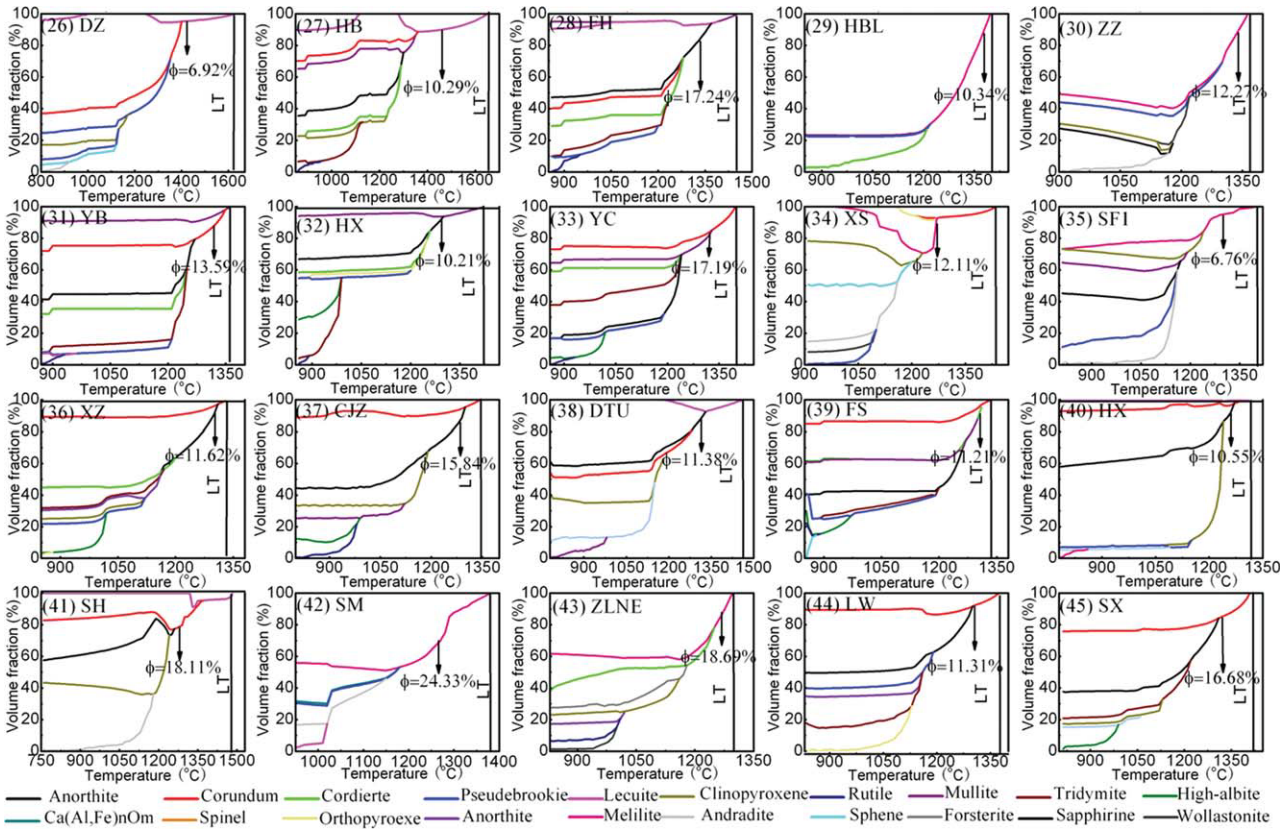

Figure 8. The volume fraction of liquid phase and crystallized solid particles and the mineral compositions for Nos. 26–45 coal ash slag samples at different temperatures.

[Color figure can be viewed in the online issue, which is available at wileyonlinelibrary.com.]

the following expression has been developed to describe the global B-value for the system with five modifiers:

$$B = \sum_{i=0}^{3} b_i^0 X_g^i + \sum_{i=0}^{3}\sum_{j=1}^{2}\left(b_i^{C,j}\frac{X_C}{X} + b_i^{M,j}\frac{X_M}{X} + b_i^{K,j}\frac{X_K}{X} + b_i^{N,j}\frac{X_N}{X} + b_i^{T,j}\frac{X_T}{X}\right) \times \left(\frac{X}{X+X_A}\right)^j X_S^i \quad (8)$$

where

$$X = X_C + X_M + X_K + X_N + X_T \quad (9)$$

where X_A, X_C, X_M, X_K, X_N, X_T, X_S are mole fractions of Al_2O_3, CaO, SiO_2, MgO, K_2O, Na_2O, TiO_2, and SiO_2, respectively; X is the sum of the mole fractions of CaO, SiO_2, MgO, K_2O, Na_2O, and TiO_2; $b_i^{C,j}$, $b_i^{M,j}$, $b_i^{K,j}$, $b_i^{N,j}$, and $b_i^{T,j}$ are empirical parameters determined through optimization—fitting the model predictions to the experimental data. The final set of B-coefficients is given in Table 2. Meanwhile, for the parameters m and n, we still used Urbain's recommended average values $m = 0.29$ and $n = 11.57$ for the 45 coal ash slag samples.

Figure 4 shows comparisons of measured values of viscosity for fully liquid phase coal ash slag samples, and the values predicted by the Urbain model and the present model (modified Urbain model) (Eqs. 4–9). As shown in Figure 4, both standard deformation (SD) value and standard error (SE) value for the present homogenous model are clearly lower than that for the Urbain model. Meanwhile, most of the coal ash slag samples shows deformation viscosities predicted by the present homogenous model within ±10% experimental error band shown, which indicates that modifying the set of B-coefficients has enabled the agreement between the model predictions and experimental viscosities to be significantly improved on the basis of the Urbain model.

Development of the Viscosity Model for Heterogeneous Coal Ash Slag. When the temperature of coal ash slag is below the liquidus temperature, solid crystallized particles will be formed in liquid coal ash slag; the liquid coal ash slag can then be regarded as a heterogeneous crystal suspension that consists of a mixture of fully liquid silicate and solid crystals.

Figures 5 and 6 illustrate the viscosity as a function of temperature and the shear rate for 45 coal ash slag samples. The viscosity of coal ash slag samples has considerable dependence on temperature. The viscosities for all the coal ash slag samples initially increase slowly, and then abruptly increase as the temperature is decreased. Meanwhile, as shown in Figures 5 and 6, the effect of shear rate on the viscosity of coal ash slag samples becomes more and more distinct as the temperature is decreased. For example, the viscosities of these samples at higher temperature, which is higher than the temperature indicated by arrows, are

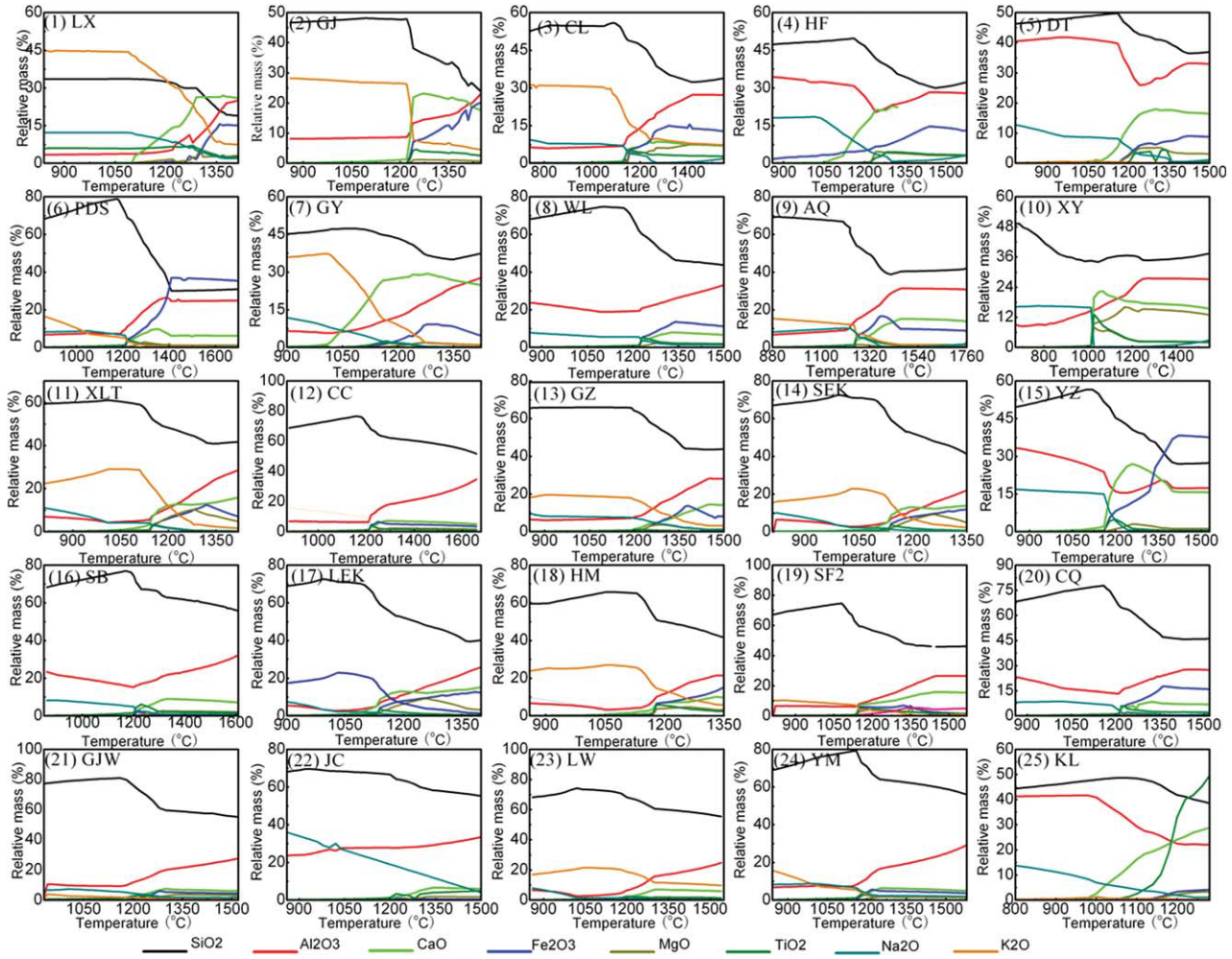

Figure 9. The composition of remaining homogeneous liquid of Nos. 1–25 coal ash slag samples at different temperatures.

[Color figure can be viewed in the online issue, which is available at wileyonlinelibrary.com.]

essentially constant regardless of the shear rate; thus it is assumed that the behavior of the heterogeneous coal ash slag samples is that of the Newtonian fluid at these temperatures. However, the viscosities of coal ash slag samples are not constant at the same temperature as the temperature is decreased, and these viscosities decrease dramatically at the same temperature with increasing shear rate (this behavior, known as "shear thinning," is common with polymer melts and particulate suspensions), thus it is assumed that the behavior of the heterogeneous coal ash slag samples is that of a non-Newtonian fluid at these temperatures. Hence, the arrows in Figures 5 and 6 indicate the temperatures which mark the transition from Newtonian to non-Newtonian behavior.

To find the critical values of solid content that marks the transition from Newtonian to non-Newtonian behavior; we used FactSage to calculate the volume fraction of crystallized solid particles for the 45 coal ash slag samples as a function of temperature. Figures 7 and 8 show the volume fraction of crystallized solid particles, liquid phase, and the mineral compositions for the 45 coal ash samples as a function of temperature. The arrows in Figures 7 and 8 corresponding to temperatures are equal to the arrows in Figures 5 and 6 corresponding to temperatures which mark the transition from Newtonian to non-Newtonian behavior for each coal ash slag samples.

By analyzing the arrows pointing to the temperatures in Figures 5 and 6 corresponding to volume fraction of crystallized solid particles in Figures 7 and 8, it is observed that for most of the coal ash slag samples, expect with LEK(17), JC(22), DZ(26), and SF1(35) of coal ash slag samples, the volume fraction of equal crystals that marks the transition from Newtonian to non-Newtonian behavior is higher than 10 vol %; meanwhile most of the values of volume fraction for these sample are close to 10 vol %, thus in our work, the critical value of volume fraction of crystallized solid particles that marks the transition from Newtonian to non-Newtonian behavior is defined as 10 vol %. As this critical value may be dependent on factors such ash crystal shape, crystal size distribution, and shear strain rate, it is only a probable value and not an exact value for coal ash slag samples.[53]

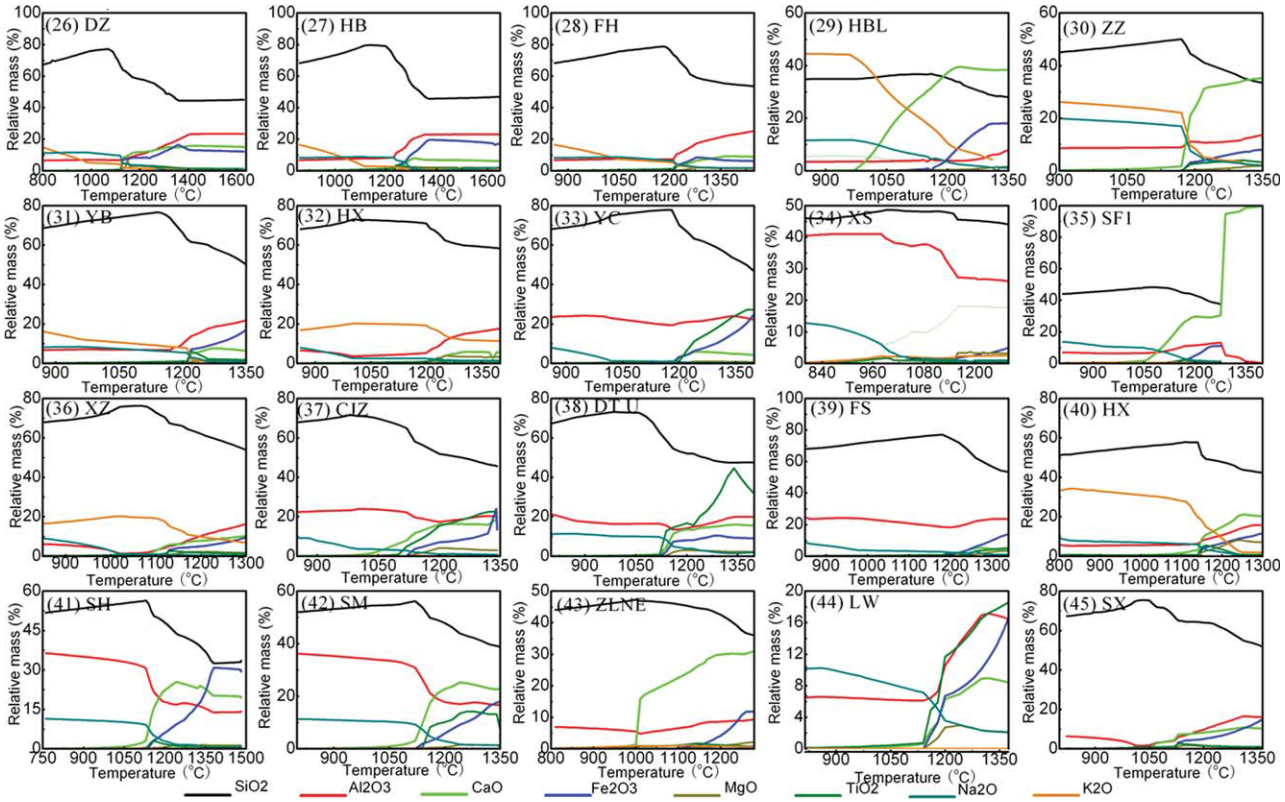

Figure 10. The composition of remaining homogeneous liquid of Nos. 26–45 coal ash slag samples at different temperatures.

[Color figure can be viewed in the online issue, which is available at wileyonlinelibrary.com.]

To describe changes in the viscosity over the entire range of crystallized particle volume fractions between $0 < \phi \leq 48.62\%$, we discuss the viscosity of coal ash slag samples of $\phi < 10.00$ vol % and $\phi \geq 10.00$ vol %, respectively.

$\phi < 10.00$ vol %.

From an inspection of Figures 5–8, when the temperature is higher than $\phi < 10$ vol % corresponding to the temperature, the effect of shear rate on the viscosity at the same temperature can be negligible. Therefore, $\phi < 10$ vol % corresponds to the viscosity of coal ash slag samples, which is assumed to be dilute silicate suspension with independent shear rate.

The most well-known method for predicting the viscosity of dilute suspension is the equation for the relative viscosity η_R, theoretically derived by Einstein on the basis of an infinitely dilute solution of spherical particles.[54]

$$\frac{\eta_s}{\eta_l} = 1 + 2.5\phi \tag{10}$$

where η_s and η_l are the viscosities of heterogeneous and remaining homogeneous liquid, respectively; ϕ is volume fraction of solids; and 2.5 is the intrinsic viscosity.

The value of the intrinsic viscosity in Eq. 10 depends on the shape and size of particles in suspension.[55] However, in our present work, the crystalline particles were not the same size of the spherical particles (see Figure 14). Moreover, the viscosity of homogenous silicate liquid in coal ash slag samples would change as the temperature is decreased, thus the value of intrinsic viscosity in the Einstein model needs to be recalculated.

First, for the viscosity value of the remaining homogeneous liquid phase in coal ash slag η_l in Eq. 10, since the composition of the remaining homogenous liquid phase of 45 coal ash slag samples are changed with temperature decreasing, its value is not constant. Therefore, in our work, the composition of the homogenous 45 coal ash slag were initially calculated by FactSage (see Figures 9 and 10), then the viscosity of the remaining homogeneous liquid slag at different temperatures coal ash slag was calculated by the present homogenous coal ash slag viscosity model (Eqs. 4–9) (see Figures 11 and 12). Then, the ϕ values for the 45 coal ash slag samples are calculated by FactSage (see Figures 7 and 8)

Figure 13 shows the relative viscosity of the solid-containing heterogeneous coal ash slag samples plotted vs. the volume fraction (<10.00 vol %) of crystallized particles. The slope of the fitting linear is the intrinsic viscosity, its value is 1.158. Thus, the modified Einstein model can be expressed through the following equation:

$$\frac{\eta_s}{\eta_l} = 1 + 1.158\phi \tag{11}$$

It can be seen in Figure 13 that there is a good correlation between η_s/η_l and ϕ, for which the correlation coefficient (R) value is higher than 0.93, and the intrinsic viscosity in Eq. 11 is lower than the value of intrinsic viscosity in the

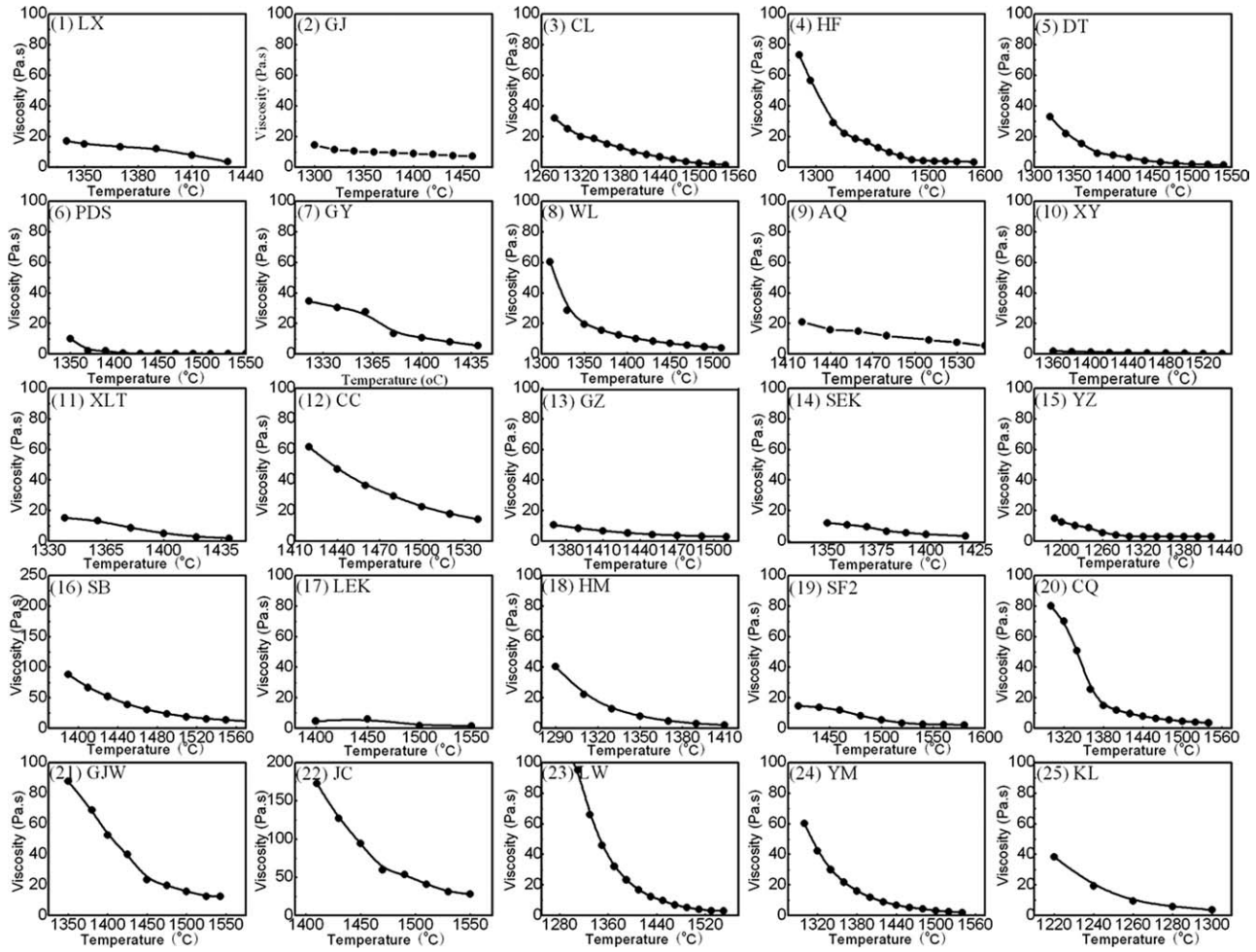

Figure 11. The viscosity values of the remaining homogenous liquid of Nos. 1–25 coal ash slag samples at different temperatures.

[Color figure can be viewed in the online issue, which is available at wileyonlinelibrary.com.]

Einstein model. One possible reason is that the viscosity of homogenous silicate liquid in most of the coal ash slag samples clearly increases as the temperature is decreased, which leads to the decrease in the value of η_s/η_l, making it lower than that of the remaining liquid viscosity which is constant. The other possible reason for the effect was that the crystallized particles in coal ash slag samples had nonspherical shapes, and in fact, they were quite irregular, which can be seen from Figure 14. Figure 14 shows the micrographs of four directly cold water quenched coal ash slag samples [LX (1), XY (10), SB (16), and KL (25)] at different temperatures from the sampling hole of the high temperature rheometer before measuring the viscosity of samples. As can be seen from Figure 14, the micrographs of coal ash slag after cooling in the water showed that the crystallized solid particles have nonspherical shape Figures 14b, c and needle-like shape Figures 14a, d.

Figure 15 shows the plot of measured viscosity vs. the predicted viscosity using the present heterogeneous model (Eq. 11) for 45 coal ash slag samples at $\phi < 10.00$ vol %. It can be seen that the present experimental viscosity data for 45 coal ash slag samples under $\phi < 10.00$ vol % are very well fitted by the modified Einstein model (Eq. 11) and most of the points lie close to the equivalence line. All of the coal ash slag samples show deformation viscosities within experimental errors of $\pm 10.00\%$.

$\phi \geq 10.00$ vol %.

From an inspection of Figures 5–8, when the temperature is lower than $\phi \geq 10$ vol % corresponding to the temperature (in Figures 7 and 8), the effect of shear rate on the viscosity at the same temperature becomes more and more distant as the temperature is decreased (in Figures 5 and 6).

Many attempts have been made to describe the concentration dependence of viscosity on high solid content suspension.[56–58] However, few authors take into account the effect of shear rate on viscosity in the model.

Coal ash slag behaves as a non-Newtonian fluid under high solid particle contents. The Einstein–Roscoe equation (Eq. 2) provides a good description of the flow properties of suspensions that contain high solid particle contents. Therefore, in our work, the Einstein–Roscoe equation was selected as the basis for the description of viscosities of coal ash slag samples at $\phi \geq 10.00$ vol %.

To make the Einstein–Roscoe equation describe the viscosity of coal ash slag at different shear rates at $\phi \geq 10.00$

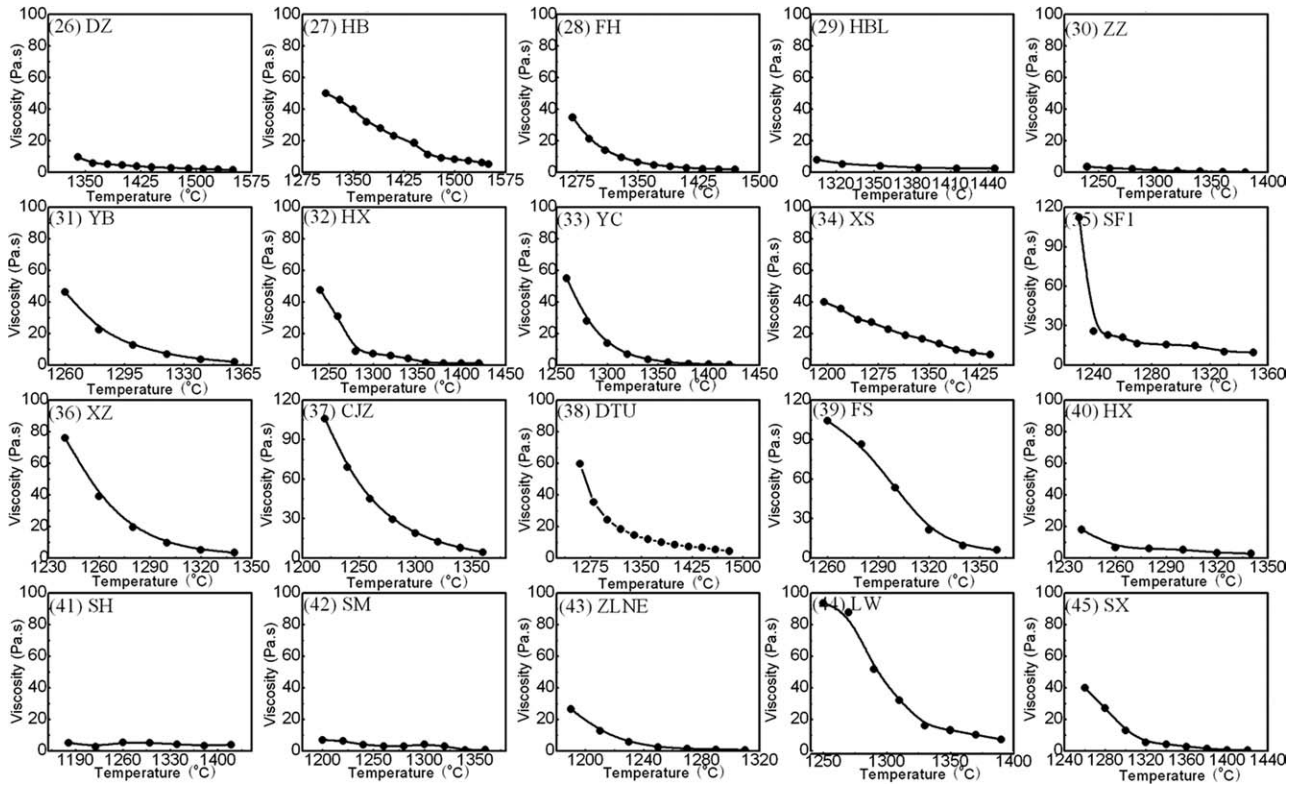

Figure 12. The viscosity values of the remaining homogenous liquid of Nos. 26–45 coal ash slag samples at different temperatures.

vol % well, the parameter D in Einstein–Roscoe equation was used as a function of shear rate. Meanwhile, the value of ϕ_m in Einstein–Roscoe equation depends on size, shape, and distribution of crystals.[59] In the literature, the values of ϕ_m range from 0.4 to 0.74,[60,61] with a classical value of 0.60 for liquid silicate suspensions.[62] In this study, the best fit to our data gives 0.62 for ϕ_m, which is sensibly higher than the classical 0.60.

The Einstein–Roscoe equation can be expressed in the form:

$$\ln\left(\frac{\eta_s}{\eta_l}\right) = D \bullet \ln\left(1-\frac{\phi}{\phi_m}\right) \tag{12}$$

Figure 16 shows the plots of relationship between $\ln(\eta_s/\eta_l)$ and $\ln(1-\phi/\phi_m)$ at different shear rate conditions. The slope of these fitting straight lines represents the value of D at different shear rates in Figure 16. As can be seen from Figure 16, all of the R values for the coal ash slag samples under different shear rates are always higher than 0.90, which indicate that there are good correlations between $\ln(\eta_s/\eta_l)$ and $\ln(1-\phi/\phi_m)$ under different shear rates conditions.

Figure 17 demonstrates the non-linear curve fit of D with shear rate, r. The relationship between the value of D in Eq. 12 and shear rate, r, is given by:

$$D = -4.62r^{-0.572} \tag{13}$$

Thus, the modified Einstein–Roscoe model can be expressed as follows:

$$\frac{\eta_s}{\eta_l} = \left(1-\frac{\phi}{\phi_m}\right)^{-4.62r^{-0.572}} \tag{14}$$

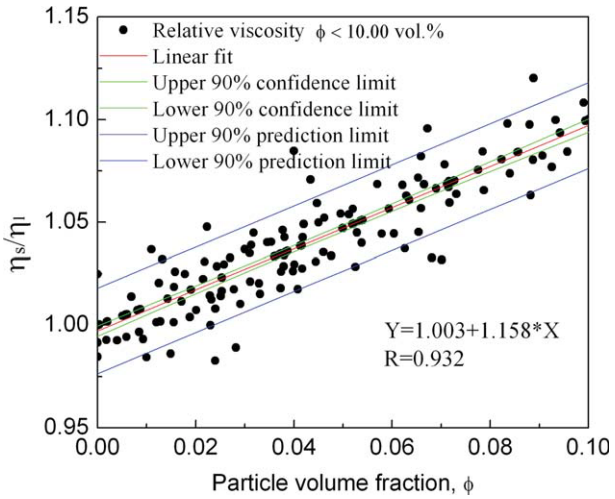

Figure 13. Relationship of relative viscosity (η_s/η_l) with volume fraction of the crystallized solid particle (ϕ) for 45 coal ash slag samples for the ϕ < 10.00 vol %.

[Color figure can be viewed in the online issue, which is available at wileyonlinelibrary.com.]

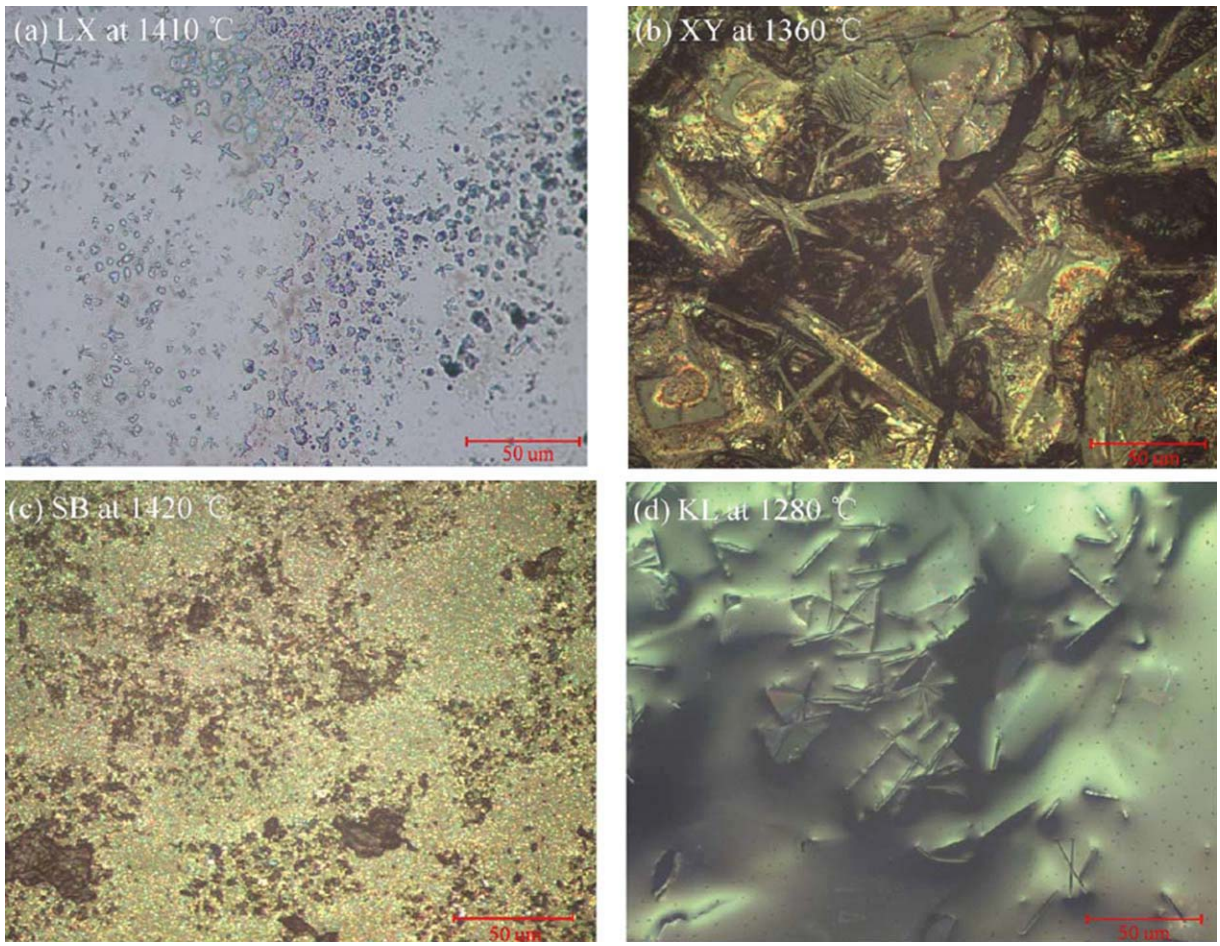

Figure 14. Micrographs of the four directly cold water quenched coal ash slag samples at different temperatures.

[Color figure can be viewed in the online issue, which is available at wileyonlinelibrary.com.]

Figure 18 shows the parity plots of the measured vs. the predicted viscosities using the present model (Eq. 13) for the 45 coal ash slag samples with different shear rates at $\phi \geq$ 10.00 vol %. It is apparent that the viscosities of most coal ash slag samples under different shear rates are observed to deform within relative errors $\pm$10%, which indicate that the modified Einstein–Roscoe model provides a good prediction of the viscosities of the 45 coal ash slag samples at $\phi \geq$ 10.00 vol % in different shear rates condition.

Application

The detailed characterization of the viscosity of coal ash at a high temperature, similar to the one performed in this article, provides essential data for the development of an effective and efficient soot blowing strategy in a pulverized coal-fired boiler. The viscosity of coal ash has significant implications in the initiation, the formation, and the growth of ash deposits in a conventional pulverized coal-fired boiler, as well as the ash deposits properties such as deposit thickness and effective thermal conductivity, which are very important factors affecting combustion regimes and operating costs.

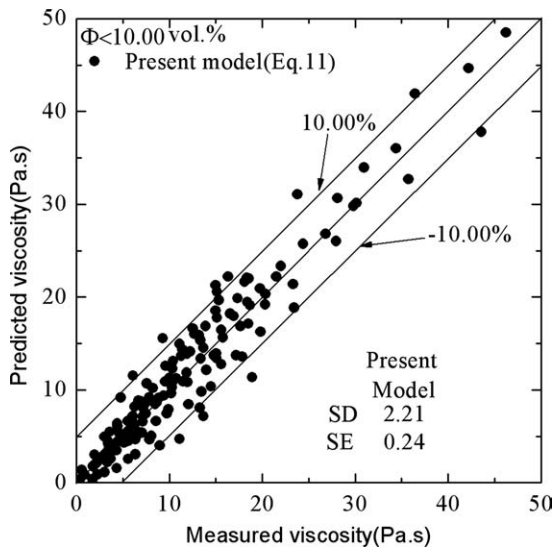

Figure 15. Comparison between the predicted viscosity values of coal ash slag samples from the present model and the experimental data at low levels of solid loading, ϕ < 10.00 vol %.

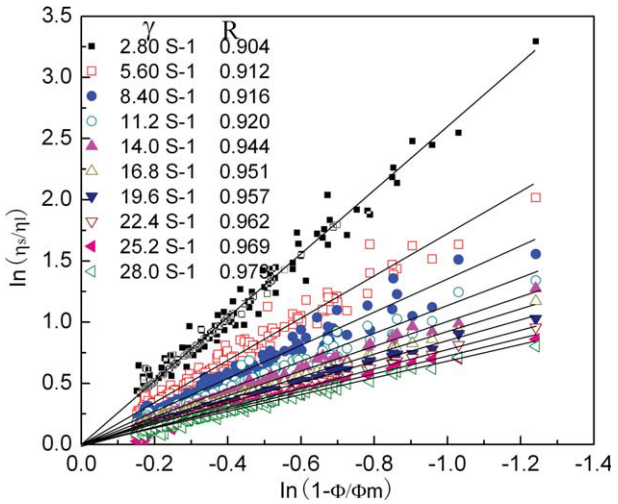

Figure 16. The relationship between $\ln(\eta_s/\eta_l)$ and $\ln(1-\phi/\phi_m)$ under different shear rates, given by Eq. 12.

[Color figure can be viewed in the online issue, which is available at wileyonlinelibrary.com.]

In practical gasification operation, depending on the gasifier type, the limiting requirements for slag viscosity and temperature can vary from 5 to 25 Pa s and from 1100°C to 1500°C, respectively.[63,64] These requirements are determined empirically by the tap ability of the slag in a gasifier. For coals with high ash fusibility temperatures and high slag viscosity, fluxing (CaO and Fe_2O_3) must be added to allow these coals to be used in the entrained gasifier to achieve required flow characteristics of ash slag in slagging gasifier.[65]

In our work, we measured the viscosities of coal ash slag samples by adding five main oxides in the coal ash slag (CaO, Fe_2O_3, MgO, SiO_2, and Al_2O_3) at different temperatures at shear rate of 14 s^{-1}; the new models then predicted the flow properties of mixtures of coal ash slag samples with CaO, Fe_2O_3, MgO, SiO_2, and Al_2O_3.

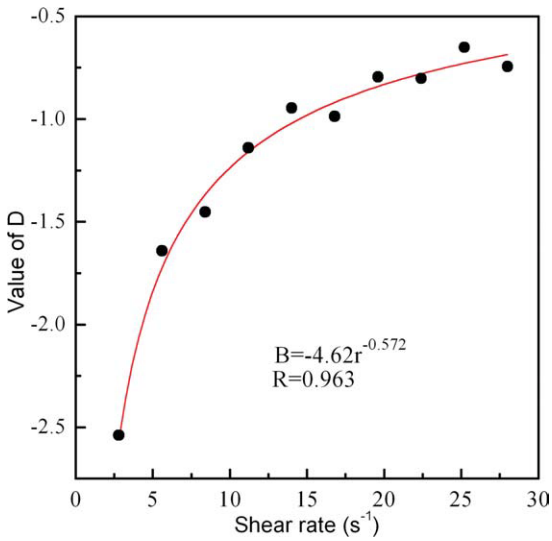

Figure 17. The relationship between value of *D* and shear rate, *r*, given by Eq. 13.

[Color figure can be viewed in the online issue, which is available at wileyonlinelibrary.com.]

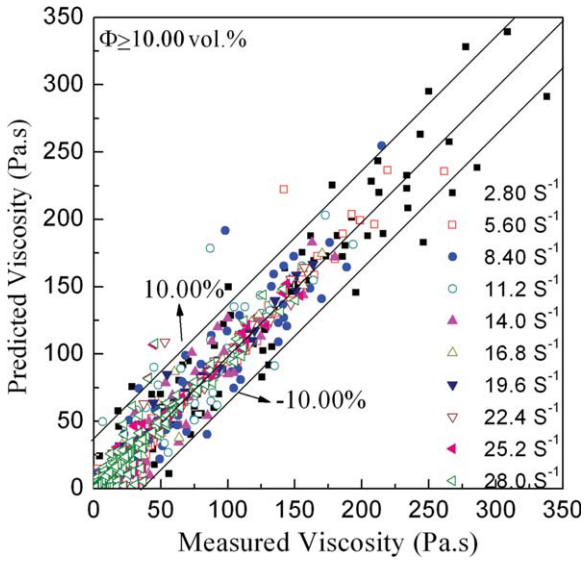

Figure 18. Comparison between measured and calculated viscosity values for 45 coal ash slag samples at higher level solid loading, $\phi \geq$ 10.00 vol %.

[Color figure can be viewed in the online issue, which is available at wileyonlinelibrary.com.]

Prediction of viscosity of mixtures of coal ash slag with various oxides

Figures 19a–d represents the measured and predicted viscosity vs. temperature curves for the mixtures of selected coal ash slag samples [GY (7), HX (40), SM (42), and ZZ (30)] with CaO, Fe_2O_3, MgO, SiO_2, and Al_2O_3, respectively. As shown in Figure 19, for most of the samples, the experimental viscosities vs. temperature curves agree well with the predictions made using the present homogenous and heterogeneous viscosity models. Table 3 shows the results of linear regression analysis for $\phi = 0$ vol %, $\phi < 10.00$ vol %, and $\phi \geq 10.00$ vol % corresponding to measured and predicted viscosity values, respectively. It can be seen that the different ϕ values corresponding to R and σ values decreases with increasing ϕ value. However, although the $\phi \geq 10.00$ vol % corresponding to R and σ values is the lowest, the R and σ values are still higher than 0.88 and 84.30%, respectively, especially for the $\phi = 0$ vol % corresponding to R and σ values which reach up to 0.931 and 91.30%, respectively. This indicates that homogenous and heterogeneous viscosity models used to predict different ϕ corresponding to viscosity of coal ash slag samples in our work can well predict the viscosity of mixtures of coal ash slag samples with different oxides.

Prediction of temperature of critical viscosity of coal ash slag

T_{cv} indicates a point of often abrupt change in the viscosity–temperature relationship because solid phases in the liquid slag

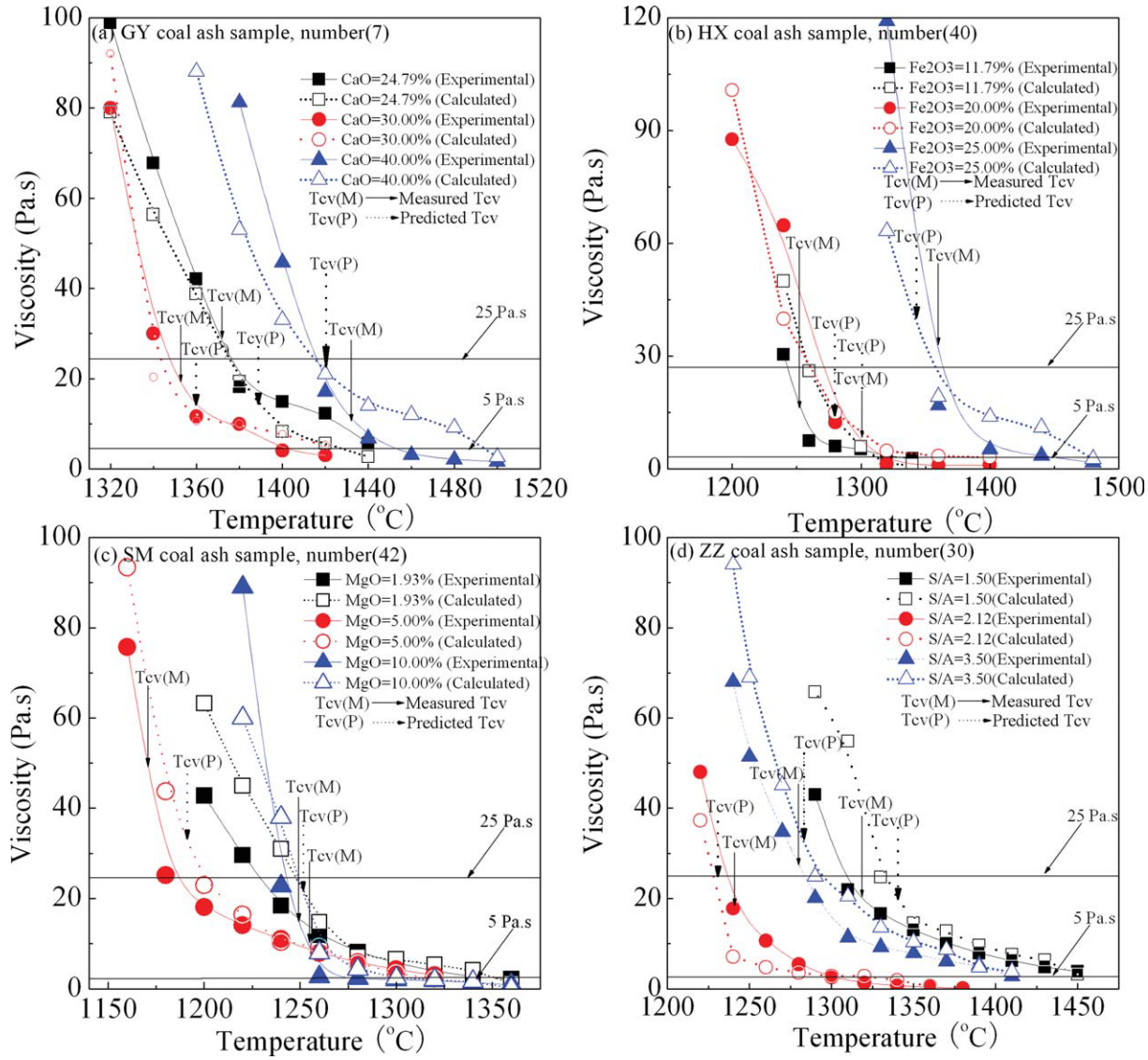

Figure 19. The measured and predicted viscosity vs. temperature curves for the mixtures of selected coal ash slag samples with CaO, Fe_2O_3, MgO, SiO_2, and Al_2O_3, respectively.

[Color figure can be viewed in the online issue, which is available at wileyonlinelibrary.com.]

begin to crystallize and separate from the liquid phase.[66] In our work, the measured and predicted T_{cv} were determined to be at the midpoint of the temperature step during which sharp breaks in the viscosity vs. temperature curve occurred. Meanwhile, the homogenous and heterogeneous models were used to predict the T_{cv} of the mixtures of selected coal ash slag with CaO, Fe_2O_3, MgO, SiO_2, and Al_2O_3, respectively.

Table 3. The Results of Linear Regression Analysis for Measured and Predicted Viscosity of Mixtures of Coal Ash Slag Samples with CaO, Fe_2O_3, MgO, SiO_2, and Al_2O_3, Respectively

Volume Fraction	Linear Regression Analysis
$\phi = 0$ vol %	$R = 0.931$, $\sigma = 91.30$ % Estimated viscosity; 89% within $< \pm 10\%$
$\phi < 10$ vol %	$R = 0.910$, $\sigma = 89.30$ % Estimated viscosity; 88% within $< \pm 10\%$
$\phi \leq 10$ vol %	$R = 0.884$, $\sigma = 84.30$ % Estimated viscosity; 83% within $< \pm 10\%$

Figure 20 shows a parity plot of the measured T_{cv} vs. the predicted T_{cv} for the mixtures of coal ash samples with these five oxides. It can be seen that all the samples show deformation temperatures within experimental errors of $\pm 25°C$,[67] which indicates that the present homogenous and heterogeneous models can predict T_{cv} of mixtures of coal ash samples with oxides with a good level of accuracy.

Conclusion

In our work, the three different viscosity models used to predict the different solid contents for 45 coal ash samples corresponding to viscosities that have been developed well describes the experimental viscosities for a wide range of

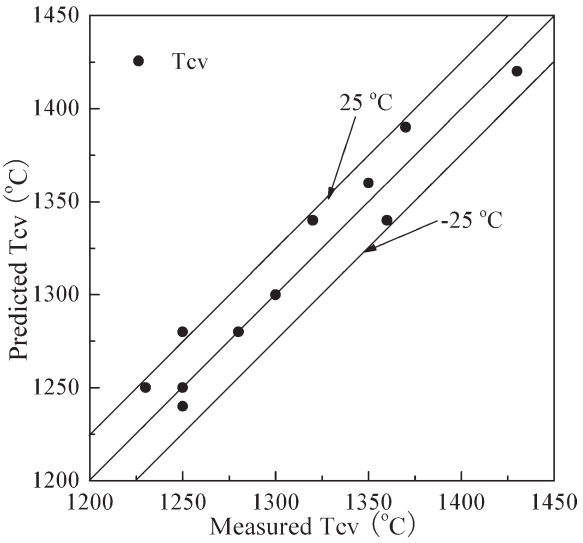

Figure 20. The measured and predicted T_{cv} for the mixtures of selected coal ash slag samples with CaO, Fe_2O_3, MgO, SiO_2, and Al_2O_3, respectively.

compositions and temperatures. Modifications to the Urbain viscosity model of the liquid phase have improved the agreement with experimental data. The viscosities of heterogeneous, partly crystallized, the Einstein equation, and Einstein–Roscoe equation have been modified to describe the viscosities of heterogeneous coal ash slags of $\phi < 10.00$ vol % and $\phi \geq 10.00$ vol %, respectively. These models provide a good description of the experimental data of fully liquid and crystallized particles coal ash slag samples. These models can also predict well the viscosity and T_{cv} of mixtures of coal ash slag samples with CaO, Fe_2O_3, MgO, SiO_2, and Al_2O_3 and described the effects of these oxides on the curves of viscosity vs. temperatures of the samples.

Acknowledgments

The authors thank Prof. Lihua Tang, Prof. Xuedong Zhu of East China University of Science and Technology (ECUST), and Prof. Yoshihiko Ninomiya of Chubu University for their valuable suggestions. The author would also like to express gratitude to other members who also contributed and helped in this research program, including Ms Xiaofen Gu and Ms Yanpin Gu. Special thanks to Assoc. Prof. Qi Zhang for support, valuable discussions and sustained encouragement. The constructive reviews and comments of two referees and the journal editor are deeply appreciated.

Notation

Subscripts

am = amphoteric oxides
A = Al_2O_3
C = CaO
F = Fe_2O_3
g = glass formers
K = K_2O
l = Liquid
M = MgO
mo = Modifiers
N = Na_2O
S = SiO_2
T = TiO_2

Superscripts

C = CaO
K = K_2O
M = MgO
N = Na_2O
T = TiO_2

Literature Cited

1. Key World Energy Statistics. International Energy Agency; Paris. 2009:24. http://www.iea.org/textbase/nppdf/free/2009/key_stats_2009.pdf.
2. International Energy Outlook. Energy Information Administration: Washington, DC. 2009:49–54. (http://www.eia.doe.gov/oiaf/ieo/pdf/0484(2009).pdf).
3. Wu HW, Li X, Hayashi J, Chiba T, Li C. Effects of volatile-char interactions on the reactivity of chars from NaCl-loaded Loy Yang brown coal. *Fuel*. 2005;84:1221–1228.
4. Fan LS, Jadhav RA. Clean coal technologies: OSCAR and CARBONOX commercial demonstrations. *AIChE J*. 2002;48:2115–2123.
5. Wee HL, Wu H, Zhang DK, French D. The effect of combustion conditions on mineral matter transformation and ash deposition in a utility boiler fired with a sub-bituminous coal. *Proc Combust Inst*. 2005;30:2981–2989.
6. Wee HL, Wu H, Zhang DK. Heterogeneity of ash deposits formed in a utility boiler during PF combustion. *Energy Fuels*. 2007;21:441–450.
7. Integrated Gasification Combined Cycle. Available at: www.IntegratedGasificationCombinedCycle.com.
8. Beer JM. Combustion technology developments in power generation in response to environmental challenges. *Progr Energy Combust Sci*. 2000;26:301–327.
9. Higman C, Van Der Burgt M. *Gasification*, 2nd ed. Boston: Elsevier/Gulf Professional Publishing Publications, 2008.
10. Buhre BJP, Browning GJ, Gupta RP, Wall TF. Measurement of the viscosity of coal-derived slag using thermomechanical analysis. *Energy Fuels*. 2005;19:1078–1083.
11. Song W, Tang L, Zhu X, Wu Y, Rong Y, Zhu Z, Koyama S. Fusibility and flow properties of coal ash and slag. *Fuel*. 2009;88:297–304.
12. Ely FG, Barnhart DH. *Coal ash: its effect on boiler availability*. In: Lowry HH, editor. *Chemistry of Coal Utilization*. NewYork: Wiley, Inc., 1963:821–891.
13. Groen JC, Brooker DD, Welch PJ, Oh MS. Gasification slag rheology and crystallization in titanium-rich, iron-calcium-aluminosilicate glasses. *Fuel Process Technol*. 1998;56:103–127.
14. Bryers RW. Fireside slagging, fouling, and high-temperature corrosion of heat-transfer surface due to impurities in steam-raising fuels. *Progr Energy Combust Sci*. 1996;22:29–120.
15. Forsbacka L, Holappa L, Iida T, Kita Y, Toda Y. Experimental study of viscosities of selected CaO–MgO–Al2O3–SiO2 slags and application of the Iida model. *Scand J Metallurgy*. 2003;32:273–280.
16. Nowok JW. Viscosity and phase transformation in coal ash slags near and below the temperature of critical viscosity. *Energy Fuels*. 1994;8:1324–1336.
17. Nowok JW. Viscosity and structural state of iron in coal ash slags under gasification conditions. *Energy Fuels*. 1995;9:534–539.
18. Jak E, Degterov S, Hayes PC, Pelton AD. Thermodynamic modelling of the system Al2O3–SiO2–CaO–FeO–Fe2O3 to predict the flux requirements for coal ash slags. *Fuel*. 1998;77:77–84.
19. Folkedahl BC, Schobert HH. Effects of atmosphere on viscosity of selected bituminous and low-rank coal ash slags. *Energy Fuel*. 2005;19:208–215.
20. Arvelakis S, Folkedahl B, Dam-Johansen KD, Hurley J. Studying the melting behavior of coal, biomass, and coal/biomass ash using viscosity and heated stage XRD data. *Energy Fuels*. 2006;20:1329–1340.
21. Shaw HR. Viscosity of magmatic silicate liquids: an empirical method of prediction. *Am J Sci*. 1972;272:870–893.
22. Senior CL, Srinivasachar S. Viscosity of ash particles in combustion systems for prediction of particle sticking. *Energy Fuels*. 1995;9:277–283.

23. Hurst HJ, Patterson JH, Quintanar A. Viscosity measurements and empirical predictions for some model gasifier slags-II. *Fuel*. 2000; 79:1797–1799.
24. Browning GJ, Bryant GW, Hurst HJ, Lucas JA, Wall TF. An empirical method for the prediction of coal ash slag viscosity. *Energy Fuels*. 2003;17:731–737.
25. Weymann HD. Temperature dependence of viscosity. *Kolloid Z Z Polymer*. 1962;181:131–137.
26. Urbain G. Viscosity estimation of slags. *Steel Res*. 1987;58:111–116.
27. Kondratiev A, Jak E. Review of experimental data and modeling of the viscosities of fully liquid slags in the Al2O3–CaO–"FeO"–SiO2 system. *Metallurg Mater Trans B*. 2001;32B:1015–1025.
28. Kondratiev A, Jak E. Predicting coal ash slag flow characteristics. *Fuel*. 2001;80:1989–2000.
29. Hurst HJ, Novak F, Patterson JH. Viscosity measurements and empirical predictions for fluxed Australian bituminous coal ashes. *Fuel*. 1999;78:1831–1840.
30. Zhang L, Jahanshahi S. Review and modeling of viscosity of silicate melts: Part I viscosity of binary and ternary silicates containing CaO, MgO, and MnO. *Metallurg Mater Trans B*. 1998;29B:177–186.
31. Zhang L, Jahanshahi S. Review and modeling of viscosity of silicate melts: Part II. Viscosity of melts containing iron oxide in the CaO–MgO–MnO–FeO–Fe2O3–SiO2 system. *Metallurg Mater Trans B*. 1998;29B:187–195.
32. Seetharaman S, Sichen D. Viscosities of high temperature systems: a modeling approach. *ISIJ Int*. 1997;37:109–118.
33. Kondratiev A, Jak E. A quasi-chemical viscosity model for fully liquid slags in the Al2O3–CaO–"FeO"–SiO2 system. *Metallurg Mater Trans B*. 2005;36B:623–638.
34. Mills KC, Chapman L, Fox AB, Sridhar S. "Round robin" project on the estimation of slag viscosities. *Scand J Metallurgy*. 2001;30: 396–403.
35. Watt JD. The flow properties of slags formed from the ashes of British coals: Part 2. The crystallizing behavior of the slags. *J Inst Fuel*. 1969;42:131–134.
36. Mills KC, Rhine JM. The measurement and estimation of the physical properties of slags formed during coal gasification. *Fuel*. 1989; 68:193–200.
37. Bottinga Y, Weill DF. The viscosity of magmatic silicate liquids: a model calculation. *Am J Sci*. 1972;272:438–475.
38. Caricchi L, Burlini L, Ulmer P, Gerya T, Vassalli M, Papale P. Non-Newtonian rheology of crystal-bearing magmas and implications for magma ascent dynamics. *Earth Planet Sci Lett*. 2007;264: 402–419.
39. Bournonville B, Nzihou A. Rheology of non-Newtonian suspensions of fly ash: effect of concentration, yield stress and hydrodynamic interactions. *Powder Technol*. 2002;128:148–158.
40. Einstein A. A Eine neue Bestimmung der Molekiildimensionen. *Ann Phys*. 1906;19:289–306.
41. Roscoe R. The viscosity of suspensions of rigid spheres. *Br J Appl Phys*. 1952;3:267–269.
42. Wright S, Zhang L, Sun S, Jahanshahi. Viscosity of a CaO–MgO–Al2O3–SiO2 melt containing spinel particles at 1646 K. *Metallurg Mater Trans B*. 2000;31B:97–104.
43. Seetharaman S, Mukai K, Du S. Viscosities of slags-an overview. *Steel Res Int*. 2005;76:267–278.
44. Oh MS, Brooker DD, de Paz EF, Brady JJ, Decker TR. Effect of crystalline phase formation on coal slag viscosity. *Fuel Process Technol*. 1995;44:191–199.
45. Bale CW, Chartrand P, Degterov SA, Eriksson G, Hack K, Mahfoud RB, Melancon J, Pelton AD, Petersen S. FactSage thermochemical software and databases. *Calphad*. 2002;26:189–228.
46. Song WJ, Tang LH, Zhu XD, Wu YQ, Zhu ZB, Koyama S. Effect of coal ash composition on ash fusion temperatures. *Energy Fuels*. DOI: 10.1021/ef900537m.
47. Song WJ, Tang LH, Zhu XD, Wu YQ, Zhu ZB, Koyama S. Prediction of Chinese coal ash fusion temperatures in Ar and H2 atmospheres. *Energy Fuels*. 2009;23:1990–1997.
48. Zhang L, Ito M, Sato A, Ninomiya Y. Fate of alkali elements during pyrolysis and combustion of Chinese coals. *J Chem Eng Jpn*. 2003; 36:759–768.
49. Watt JD. Fereday F. The flow properties of slags formed from the ashes of British coals: Part 1. Viscosity of homogeneous liquid slags in relation to slag composition. *J Inst Fuel*. 1969;42:99–103.
50. Urbain G, Boiret M. Viscosities of liquid silicates. *Ironmaking Steelmaking*. 1990;17:255–260.
51. Urbain G, Cambier F, Deletter M, Anseau MR. Viscosity of silicate melts. *Trans J Br Ceram Soc*. 1981;80:139–141.
52. Mills KC. *Viscosities of Molten Slags*. Berlin: Springer-Verlag, 1995.
53. Ishibashi H, Sato H. Viscosity measurements of subliquidus magmas: alkali olivine basalt from the Higashi-Matsuura district, Southest Japan. *J Volcanol Geothermal Res*. 2007;160:223–238.
54. Einstein A. Eine neue bestimmung der moleküldimensionen. *Annalen der Physik*. 1911;34:591–592.
55. Vand V. Viscosity of solution and suspensions. *J Phys Colloid Chem*. 1948;52:277–299.
56. Champallier R, Bystricky M, Arbaret L. Experimental investigation of magma rheology at 300 MPa: from pure hydrous melt to 76 vol % of crystals. *Earth Planet Sci Lett*. 2008;267:571–583.
57. Lejeune AM, Richet P. Rheology of crystal-bearing silicate melts: an experimental study at high viscosities. *J Geophys Res*. 1995;100: 4215–4229.
58. Usui H, Kishimoto K, Suzuki H. Non-Newtonian viscosity of dense slurries prepared by spherical particles. *Chem Eng Sci*. 2001;56: 2979–2989.
59. Chong JS, Christiansen EB, Baer AD. Rheology of concentrated suspensions. *J Appl Polym Sci*. 1971;15:2007–2021.
60. Jeffrey DJ, Acrivos A. The rheological properties of suspensions of rigid particles. *AIChE J*. 1976;22:417–432.
61. Donev A, Cisse I, Sachs D, Variano EA, Stillinger FH, Connelly R, Torquato S, Chaikin PM. Improving the density of jammed disordered parkings using ellipsoids. *Science*. 2004;303:990–993.
62. Marsh DB. On the crystallinity, probability of occurrence, and Rheology of lava and magma. *Contrib Mineral Petrol*. 1981;78:85–98.
63. Patterson JH, Hurst HJ. Slag Characteristics of Australian Bituminous Coals for Utilization in Slagging Gasifiers, Proceedings of workshop "Impact of coal quality on thermal coal utilization." Brisbane, Australia: CRC Black Coal Utilisation, 1996.
64. Harris DJ, Patterson JH. Use of Australian bituminous coals in IGCC power generation technologies. *Aust Inst Energy News*. 1995; 13:22–32.
65. Bryant GW, Lucas JA, Gupta SK, Wall TF. Use of thermomechanical analysis to quantify the flux additions necessary for slag flow in slagging gasifiers fired with coal. *Energy Fuels*. 1998;12:257–261.
66. Vargas S, Frandsen FJ, Dam-Johansen K. Rheological properties of high-temperature melts of coal ashes and other silicates. *Progr Energy Combust Sci*. 2001;27:237–429.
67. Seggiani M. Empirical correlations of the ash fusion temperatures and temperature of critical viscosity for coal and biomass ashes. *Fuel*. 1999;78:1121–1125.

Manuscript received Nov. 30, 2009, and revision received Apr. 22, 2010.